acta physica slovaca vol. 44 No. 4/5, 245 – 260 August 1994

ADSORBED MONOLAYERS: PHASE TRANSITIONS AND QUANTUM EFFECTS[1]

Peter Nielaba[2]
Institut für Physik, KoMa 331, Universität Mainz D–55099 Mainz, Germany

Received 12 April 1994, accepted 2 May 1994

Phase transitions in adsorbed (two dimensional) fluids and in adsorbed layers of linear molecules are studied with a combination of path integral Monte Carlo (PIMC), Gibbs ensemble Monte Carlo and finite size scaling techniques. For a classical (non additive) hard disc fluid the "critical" non-additivities, where the entropy driven phase separations set in, are presented. For a fluid with internal quantum states the gas-liquid coexistence region, tricritical- and triple points can be determined, a comparison with density functional (DFT) results shows good agreement for the freezing densities. Linear N2 molecules adsorbed on graphite (in the $\sqrt{3} \times \sqrt{3}$ structure) show a transition from a high temperature phase to a low temperature phase with *herringbone* ordering of the orientational degrees of freedom. The order of the transition is determined in the anisotropic planar rotor model by analysis of the correlation length ξ near the transition temperature T_0. The simulation data, extrapolated to T_0, yield a large but finite ξ at T_0 demonstrating that the herringbone ordering is a weak first order transition. The effect of quantum fluctuations on the herringbone transition is quantified by PIMC and classical simulational methods. Quasiclassical and quasiharmonic calculations agree for high and low temperatures, respectively, but only PIMC gives satisfactory results over the entire temperature range. Rounding effects of the phase transition in adsorbed layers of $(N2)_x$ $(CO)_{1-x}$ for $x < 7\%$ are analyzed by Monte Carlo methods, the ground state ordering for the transition in the adsorbed pure CO system is discussed, using ab initio potentials.

I. Introduction

Two dimensional (2D) layers at surfaces have become an interesting field of research during the last decade [1, 2, 3]. Most of the phase transitions in these systems occur at fairly low temperatures, and for many aspects of the behavior, quantum effects need to

[1] Invited lecture at MECO (Middle European CoOperation) 19, Smolenice, Slovakia, April 11-15, 1994

[2] e-mail address: nielaba@vipmza.physik.uni-mainz.de

0323-0465/94

be considered. This holds in particular if one is concerned with adsorbed molecules at surfaces, since the molecules have internal degrees of freedom which need to be treated quantum - mechanically even if the translational degrees of freedom can still be treated classically.

In section II we study the properties of model fluids in two spatial dimensions with Gibbs ensemble Monte Carlo (GEMC) techniques. In particular in section II A we study the entropy driven phase separation in case of a nonadditive symmetric hard disc fluid and locate by a combination of GEMC with finite size scaling techniques the critical line of nonadditivities as a function of the system density, which separates the mixing/demixing regions, we compare with a simple approximation. In section II B we successfully combine path integral Monte Carlo (PIMC) and GEMC techniques in order to locate the gas–liquid coexistence densities for a fluid with classical degrees of freedom and internal quantum states, a comparison with NVT-ensemble results and mean field predictions is presented, in section II C a density functional approach is outlined. Linear N_2 molecules adsorbed on graphite (in the $\sqrt{3} \times \sqrt{3}$ structure) show a transition from a high temperature phase to a low temperature phase with *herringbone* ordering of the orientational degrees of freedom. In section III A the order of the transition is determined in the anisotropic planar rotor model by analysis of the correlation length ξ near the transition temperature T_0. The simulation data, extrapolated to T_0, yield a large but finite ξ at T_0 demonstrating that the herringbone ordering is a weak first order transition. In section III B the effect of quantum fluctuations on the herringbone transition is quantified by PIMC and classical simulational methods. Quasiclassical and quasiharmonic calculations agree for high and low temperatures, respectively, but only PIMC gives satisfactory results over the entire temperature range. In section IV the random-field-induced rounding of the Ising–type transition in physisorbed $(CO)_{1-x}(N_2)_x$ mixtures is studied. Good qualitative agreement with recent experiments is obtained with a simple model. Summarizing conclusions are given in section V.

II. Phase Transitions in Classical and Quantum Two-dimensional Fluids

A. Phase Transitions in Nonadditive Symmetric Hard Disc Fluids

Phase transitions in systems with purely repulsive interaction have got much attention recently [4]. In this section we consider a system of hard discs (of diameter d) with N_A particles of type A and N_B particles of type B and interaction potential:

$$U(r_{12}) = \begin{cases} 0 & : \; r_{12} > d_{s_1 s_2} \\ \infty & : \; r_{12} < d_{s_1 s_2} \end{cases} \qquad (1)$$

r_{12} is the distance of two particles, $s_1, s_2 \in \{A, B\}$ are their species and $d_{AA} = d_{BB} = d$, $d_{AB} = d + \Delta/2$. The total number of particles N and the total volume V is fixed and thus the average density $\rho^* = \rho * d^2 = Nd^2/V$. Due to the additional repulsion between A and B- type particles we expect a phase separation into a A-rich and a B-rich fluid

Table 1. Critical line for nonadditive hard discs obtained by the cumulant intersection method. For the largest values of Δ_c the critical density ρ_c^* was found by density variation, the smallest critical values of Δ_c were obtained for fixed density.

ρ_c^*	Δ_c/d
0.6	0.562 ± 0.04
0.55	0.66 ± 0.01
0.5	0.789 ± 0.01
0.499 ± 0.01	0.85
0.5 ± 0.02	0.9
0.508 ± 0.03	0.95
0.46 ± 0.02	1

phase for large values of $\Delta > \Delta_c$ and fixed total density. For $\Delta = 0$ we have a pure hard disc fluid with no phase separation in the fluid phase. In order to locate the critical values Δ_c as a function of ρ^* we perform GEMC simulations [5]. Since the phase separation is driven by entropy we expect only a small interfacial free energy in case of phase coexistence. In order to be able to locate the critical points even in such extreme situations we combine the GEMC with the block analysis finite size scaling techniques [5]. The GEMC results [7, 8] were obtained with N=512 particles and about 10^6 Monte Carlo steps, where each step consisted of 400 attempted moves, 20 particle exchange and 2 volume change attempts. Cell occupancy lists were successfully used to speed up the procedure, the overall computing time for was about 4300 CPU hours on RISC 6000/250 workstations.

In order to get a rough idea about the critical line l_c, defined by $\rho_c^*(\Delta_c)$ we computed l_c in analogy to a study in three dimensions [9] by convex envelope arguments for the free energy and arrive at the compact expression:

$$\rho_c^*(\Delta_c) = \frac{4}{\pi}\left(1 - \sqrt{\frac{\Delta}{d+\Delta}}\right) \qquad (2)$$

The critical points were obtained by inspection of number-difference histograms $P_L(N_A - N_B)$ on different length scales L obtained by subdivision of the simulation boxes of sizes V_1 and V_2 ($V_1 + V_2 = V$) into smaller subsystems of size $L \times L$. For $\Delta < \Delta_c$ the distributions are all singly peaked, for larger Δ we obtain a single peak structure of $P_L(N_A - N_B)$ for large L and a double peak structure for small L. An analysis of these histograms with the cumulants $U_L = 1 - < (N_A - N_B)^4 >_L / 3 < (N_A - N_B)^2 >_L^2$ allows a determination of critical points, due to the cumulants L- invariance at the critical point. The GEMC results for the critical line are presented in table 1. Similarly to the prediction of eq.(2) ρ_c is a decreasing function of Δ_c, however at a given density the GEMC results for Δ_c are about 20% larger than the predictions of eq.(2).

B. Path Integral Monte Carlo Simulations in the Gibbs Ensemble

In this section we present results of a novel combination of GEMC and path integral Monte Carlo simulation techniques [7, 10]. In particular we study the gas–liquid

Table 2. Gas-liquid coexistence densities of the two-dimensional fluid with internal quantum states versus temperature. Comparison of Gibbs ensemble Monte Carlo results with those of an NVT- ensemble simulation and mean field predictions.

T^*	Gibbs- MC		NVT- MC [12]		Mean Field	
	ρ_g^*	ρ_l^*	ρ_g^*	ρ_l^*	ρ_g^*	ρ_l^*
0.35	0.139	0.739	0.174	0.711	0.198	0.762
0.4	0.196	0.715	0.232	0.659	0.240	0.744
0.45	0.265	0.685	0.298	0.639	0.276	0.726
0.5	0.323	0.633	0.341	0.576	0.3	0.702
0.55	0.376	0.521	0.399	0.506	0.324	0.684

transition of a model fluid with internal quantum states. The Hamiltonian is given by:

$$H = \sum_{i=1}^{N} \frac{\mathbf{p}_i^2}{2M} - \frac{\omega_0}{2} \sum_{i=1}^{N} \sigma_i^x + \sum_{i<j} U(r_{ij}) - \sum_{i<j} J(r_{ij}) \sigma_i^z \sigma_j^z \qquad (3)$$

M is the particle mass, $\mathbf{p}_i$ is the momentum of particle i, r_{ij} is the distance between particle i and j, σ^x and σ^z are the usual Pauli spin - 1/2 matrices. The potential energy consists of a one-particle (two-level) part $\omega_0/2$ and two pair interaction terms $U(r)$ and $J(r)$, where U is a hard disc potential for particles with diameter d and $J(r) = J$ for $d < r < 1.5\,d$ and zero elsewhere. For motivation and literature background for these type of models see refs. [11, 12]. In the adiabatic approximation (large M) we assume a separation of time scales for the translational degrees of freedom and the internal quantum states. An application of the Trotter formula results in the following expression [7, 10, 11, 12] for the partition function $Z_{N_1,V_1,T} = \lim_{P\to\infty} Z_P$ at temperature $T^* = (\beta J)^{-1}$, with

$$Z_P(\beta, N_1, V_1) = \frac{A_P^{N_1 P}}{\lambda^{2N_1} N_1!} \int d\mathbf{r}_1 \cdots \int d\mathbf{r}_{N_1} \exp\left[-\beta \sum_{i<j} U(r_{ij})\right]$$

$$\times \sum_{\{S\}} \exp[-\beta \sum_{i=1}^{N_1} \sum_{p=1}^{P} \left(K_P S_{i,p} S_{i,p+1} + \frac{1}{P} \sum_{i\neq j=1}^{N_1} J(r_{ij}) S_{i,p} S_{j,p} \right)] \qquad (4)$$

Here N_1 denotes the number of particles in one of the GEMC-boxes at volume V_1. In the GEMC simulation in addition all necessary volume and particle decompositions have to be taken into account properly for the full partition function [7, 10]. The coefficients A_P and K_P are given by

$$A_P = [\frac{1}{2}\sinh(\beta\omega_0/P)]^{1/2}, \quad K_P = \frac{1}{2\beta}\ln[\coth(\beta\omega_0/2P)]\,. \qquad (5)$$

λ is the thermal de Broglie wavelength and the quantum chains have periodic boundary conditions w.r.t. P, and $S_{i,p} = \pm 1$.

In order to study the systematic ensemble and size dependencies of the gas-liquid coexistence densities, which recently got much attention in the context of GEMC simulations [13], we chose the same interaction parameters as in ref. [12]. The Gibbs ensemble simulations [7, 10] were done with $N = 200$ particles and $P/\beta J = 40$. A typical run over 10^6 Monte Carlo steps (consisting of 200 attempted moves, 20 particle exchange and 1 volume change attempts) took about 14 CPU hours on a CRAY YMP.

In an additional study we analyzed the phase diagram by a combination of PIMC and finite size scaling techniques [12]. We obtain the phase diagram including phase coexistences, tricritical and triple points to a high degree of precision by combining block analysis finite size scaling ideas with Quantum Monte Carlo techniques. In addition, we find a *square* lattice solid phase in coexistence with gas and / or liquid phases. We observed the following general behavior: in the high temperature regime as the density is increased a second order transition from a paramagnetic (PM) to a ferromagnetic (FM) *fluid* phase takes place; we measure the magnetization in z - direction. This is equivalent to a changeover from occupation of eigenstates of σ^x to that of σ^z, i.e. hybridization occurs and the "molecules change their preferred internal state". Applying the finite size block analysis technique [6], sketched in section II A, in conjunction with the density cumulant intersection method[6] we are able to locate this tricritical point at the end of the critical line at $((\beta_{tri}J)^{-1}, \rho_{tri}R^2) = (0.57 \pm 0.02, 0.45 \pm 0.01)$. Below the tricritical temperature a PM *gas* phase coexists with a FM *liquid* phase for a certain density window.

By cooling the system further down a sudden jump in the coexistence curve on the high density side occurs: the system crystallizes into a solid phase. Below this temperature we find coexistence of a PM *gas* phase with a *square* lattice FM *solid* phase. We assume that the square lattice is stable because of the particular choice of the interaction potential $J(r)$ of the square well type, which favours square lattice structures energetically at low temperatures.

The results of the GEMC simulations for the gas-liquid coexistence densities are presented in table 2, together with the NVT- ensemble results of ref. [12] and mean field (MF) predictions. We note only a weak ensemble dependency of the results. The mean field theory predicts a too large coexistence region resulting in a 100% deviation from the GEMC results for the gas-liquid critical temperature T_c, which was found by GEMC to be about $T_c = 0.57$, in good agreement with NVT-ensemble results.

The MF study provides a qualitative correct phase diagram but it underestimates the fluctuations and in principle only contains the tricritical exponents of the system in three dimensions. The exponent describing the merging of the phase boundaries in the tricritical point is distinctly smaller than the MF value (unity) resulting in a much flatter shape of the coexistence region and thus the tricritical temperature is off by a factor of two as compared to PIMC!

C. Density functional theory

We now discuss [14] a modification of the Ramakrishnan–Yussouff theory [15] to the model fluid of section II B. We start by introducing a combined classical - quantum

free energy functional of the time averaged number density $\rho(\mathbf{r})$ and the magnetisation density $m(\mathbf{r})$ for the Helmholtz free energy per unit volume. We incorporate the magnetic interaction arising from the presence of the internal quantum states in the sense of a mean field treatment [11] of the attractive interaction in addition to the classical hard disc contribution to the free energy. The magnetization density $m(\mathbf{r})$, for the ferromagnetic solid that we consider here, is proportional to the number density, i.e. $m(\mathbf{r}) = m_0\rho(\mathbf{r})$; we measure the magnetization in the magnetic z–direction. In the mean–field model, the magnetic field on one particle due to the interaction with all other particles is approximated by the average molecular field, $\xi_m(\mathbf{r}) = \int d\mathbf{r}' m(\mathbf{r}-\mathbf{r}')J(\mathbf{r}')$. As a result the (many body) Hamiltonian (3) effectively reduces to a one–body Hamiltonian, which can be straightforwardly diagonalized. The free energy functional in this approximation is given by,

$$\beta f([\rho]) = \beta f_{cl}([\rho]) + \frac{\beta}{2}\int \frac{d\mathbf{r}}{V} m(\mathbf{r})\xi_m(\mathbf{r}) - \int \frac{d\mathbf{r}}{V}\rho(\mathbf{r})\ln[2\cosh\{\beta(\xi_m^2(\mathbf{r})+\omega_0^2/4)^{1/2}\}] \quad (6)$$

The integrals are over the full two -dimensional "volume" V. For the classical contribution to the free energy $\beta f_{cl}([\rho])$ we have used the Ramakrishnan -Yussouff functional in the form recently introduced by Ebner, Krishnamurthy and Pandit which is known[16] to reproduce accurately the phase diagram of the Lennard - Jones system in three dimensions. In the classical part of the free energy functional, we require as an input the Ornstein - Zernike direct correlation function for the hard disc fluid. For the DFT–calculations reported we have used, for this quantity, the accurate and convenient analytic form due to Rosenfeld[17].

The free energy functional (6) needs to be minimized with respect to choices of (non -uniform) densities $\rho(\mathbf{r})$ to obtain the Helmholtz free energies of the solid phases. Motivated by the simulation results, we studied in addition to the usual hexagonal also the square lattice solid. In order to obtain the free energies of the solids, we approximate the one body density $\rho(\mathbf{r})$ at position $\mathbf{r}$ by a set of non - overlapping Gaussians with width α/a^2 centered on lattice sites $\mathbf{R}$ in a lattice of lattice parameter a.

$$\rho(\mathbf{r}) = \frac{\rho_0 A_n \alpha}{a^2\pi}\sum_{\mathbf{R}} \exp[-\alpha(\mathbf{r}-\mathbf{R})^2/a^2] \quad (7)$$

where ρ_0 is the average density of the solid and A_n denotes the area of the unit cell. This ansatz for the density now reduces the free energy functional to a *function* of the variables m_0 and α. The global minimum of this function in the space of α and m_0 for a choice of $\{\mathbf{R}\}$ gives the Helmholtz free energy of the chosen lattice. Knowing the Helmholtz free energy in the fluid phase from the mean field analysis of the same system for the homogeneous case by de Smedt *et. al.*[11], it is straight forward to obtain the $T^* - \rho^*$ phase diagram by performing double tangent constructions to obtain coexistence densities.

The phase diagram of Hamiltonian (3), has the following features ($\omega_0 = 4$ and $J_0 = 1$ where chosen as in the simulation): In the high temperature limit, the system is paramagnetic for all densities and we observe the (temperature independent) hard disc freezing transition. Our estimates for the freezing density ($\rho_l^* = 0.847$) and the fractional density change during freezing ($\eta = 0.066$) are close to the estimates for the same quantities in computer simulations ($\rho_l^* = 0.878$, $\eta = 0.0499$) and previous theoretical studies ($\rho_l^* = 0.858$, $\eta = 0.0723$) of the two dimensional hard disc system, both known from the literature [14]. As the temperature is reduced below $T^* = 5.9$, the system undergoes a second order transition from a paramagnetic fluid phase at low densities to a ferromagnetic fluid at high densities and a first order transition from a ferromagnetic fluid to a ferromagnetic hexagonal solid. As expected, the freezing density decreases with decreasing temperature due to the greater stability of the solid phase arising from the magnetic interaction. The DFT–predictions for the location of the fluid–solid transition was confirmed by an anlaysis of bond–orientation order parameter of Monte Carlo data [18]. Also, the average magnetization of the solid m_0 is observed to be higher than that of the fluid. At temperatures below the tricritical point T^*_{TCP}, = 1.25, we have a first order transition from a paramagnetic gas to a ferromagnetic fluid in addition to the liquid - solid transition. The liquid phase is stable only for temperatures above a first triple temperature $T^*{}_{TP_1} = 0.55$, while for temperatures below $T^*{}_{TP_1}$ and above $T^*{}_{TP_2} = 0.07$, we obtain coexistence of a paramagnetic gas with a ferromagnetic hexagonal solid. The square lattice solid, observed in the Monte Carlo simulations[12] at $T^* = 0.16 \pm 0.01$, starts appearing at temperatures below $T^* = 0.09$ and for a range of temperatures $T^*{}_{TP2} < T^* < 0.09$ there exists a re-entrant transition with the hexagonal solid appearing for low and high densities separated by a narrow region of square solid stability centered around $\rho^* = 1.0$. Upon lowering temperatures below the paramagnetic gas - ferromagnetic square solid - ferromagnetic hexagonal solid triple point ($T^*{}_{TP_2}$), we found a gas - square solid coexistence followed by a square solid - hexagonal solid structural transition at higher densities.

The topology of our phase diagram is in agreement with our Monte Carlo results. We successfully predict a thermodynamically stable *square lattice solid*, a surprising finding in the simulation [12]. Because of second nearest neighbor contributions in the square lattice structure, resulting from the particular choice of the magnetic interaction $J(\mathbf{r})$, the square lattice has a lower magnetic energy. The hard disc contribution, however, strongly disfavors the square lattice structure in two dimensions.

III. Orientational Phase Transitions in Adsorbed Monolayers

A. The Order of the Herringbone Transition of N_2 on Graphite

Since many years adsorbed layers of N_2 on graphite serve constantly, as a prototype example to study phase transitions in two dimensions. The phase diagram [19], includes below 50 K a registered phase having a commensurate $(\sqrt{3}\times\sqrt{3})R30°$ structure. The orientations of the molecular axes undergo in this phase an *orientational* phase transition quite independent from coverage (below a coverage of 1.2) at around 27 K to the "2-in"herringbone phase keeping the translationally ordered $\sqrt{3}$ structure of the molecular centers of mass; for an overview over the experimental and theoretical literature see ref. [20, 21]. Stimulated by a controversial discussion on the order of the transition

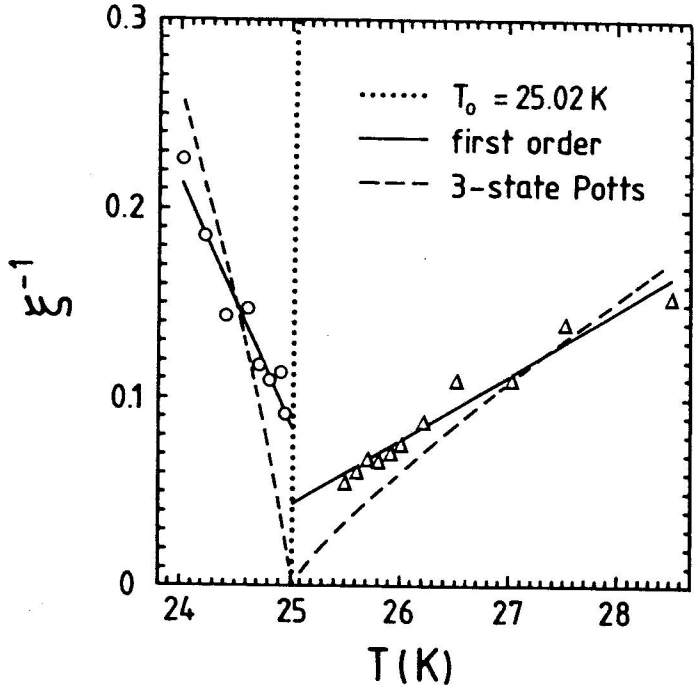

Fig. 1. Inverse effective correlation length ξ^{-1} in units of the lattice constant $a = 4.26$ Åas a function of temperature; the extrapolated transition temperature $T_0 = 25.02 \pm 0.08$ K as obtained independently from energy cumulants is marked by a dotted line. Full lines correspond to a fit assuming a simple linear dependence $\xi = \xi_{\pm} + C_{\pm} \mid 1 - T/T_0 \mid$ expected near T_0 for a first order transition, while dashed lines assume the critical behavior of the 3-state 2D Potts class, $\xi = \xi_0^{\pm} \mid 1 - T/T_0 \mid^{-\nu}$ with [26] $\nu = 5/6$ and [27] $\xi_0^+/\xi_0^- = 4.1$.

(for an overview see ref. [20]) we investigated [20] the herringbone phase transition of N_2 in the $(\sqrt{3} \times \sqrt{3})$R30° commensurate phase on graphite by large scale Monte Carlo simulations using the anisotropic planar–rotor model. The effective correlation length ξ is measured near the transition temperature T_0. The data, extrapolated to T_0, yield a large but *finite* ξ at T_0 demonstrating that the herringbone ordering is a *weak first order* transition.

Following the previous studies [22] of the order of the N_2 herringbone transition on graphite, we use the APR Hamiltonian [23]

$$H = K(\mathrm{N_2}) \sum_{\langle i,j \rangle}^{N} \cos\left[2\varphi(\mathbf{R}_i) + 2\varphi(\mathbf{R}_j) - 4\Theta_{ij}\right] \tag{8}$$

to model the quadrupolar interactions between the $N = L^2$ molecules; all angles are measured relative to one symmetry axis of the triangular lattice, and Θ_{ij} is the angle connecting lattice sites $\mathbf{R}_i$ and $\mathbf{R}_j$. The rotators $\{\varphi(\mathbf{R}_i)\}$ are pinned with their center

of mass on a triangular lattice $\{\mathbf{R}_i\}$ representing the $(\sqrt{3} \times \sqrt{3})$R30° structure, and only nearest neighbor interactions $\langle i, j \rangle$ are taken into account. The coupling constant $K(\mathrm{N_2}) = 33$ K is obtained [22, 23] from the electrostatic quadrupole moment of N_2 and the $\sqrt{3}$–lattice constant is $a = 4.26$ Å. We define correlation functions

$$\Gamma_\alpha(l) = \left\langle \frac{1}{N} \sum_{i=1}^{N} \cos\left[2\varphi(\mathbf{R}_i) + 2\varphi(\mathbf{R}_i + l\mathbf{a}_\alpha)\right] \right\rangle \tag{9}$$

along the three symmetry axes, where $\{\mathbf{a}_\alpha\}$ denotes lattice vectors ($\mid \mathbf{a}_\alpha \mid = a$) along these axis and l runs over the neighbors along these directions. Although it is known that the decay of $\Gamma_\alpha(l)$ for large distances l should be exponential, $\Gamma_\alpha(l) \propto \exp[-l/\xi]$, an estimation of ξ from simulations is difficult. For small l there may be strong systematic corrections to this law, while for large l there are not only severe statistical problems but also systematic corrections due to the periodic boundary conditions, i.e., $\Gamma_\alpha(l) = \Gamma_\alpha(L-l)$. Also, lattice structure effects such as an even–odd oscillation of $\Gamma_\alpha(l)$ present a difficulty. Thus ξ often depends on the range of l used in a fit to the exponential decay law. These problems are avoided by the procedure [24] defining ξ_l via

$$\delta_m \ln \Gamma_\alpha(l) := \ln\left[\frac{\Gamma_\alpha(l) - \Gamma_\alpha(\infty)}{\Gamma_\alpha(l+m) - \Gamma_\alpha(\infty)}\right] = \frac{m}{\xi_l} \tag{10}$$

where $\Gamma_\alpha(\infty) := \Gamma_\alpha(L/2 \gg l \gg \xi)$ denotes the constant asymptotic value of (9) which vanishes in the disordered phase; $m = 2$ takes care of the fact that $\Gamma_\alpha(l)$ oscillates with period two, see ref. [25]. The advantage of this approach is that no (possibly uncontrolled) fitting is involved, and especially that the range where ξ_l approximates the true ξ can be assessed by inspection. If a plot of $\delta_m \ln \Gamma_\alpha(l)$ versus l yields a *plateau* for a certain window of distances l then ξ may safely be extracted from such a plateau value, i.e., the linear dimension of the system and the quality of the data (equilibration, statistics) are sufficient. The simulations were carried out [20] with a standard Metropolis MC algorithm which is highly vectorized via a three sublattice checkerboard decomposition using fully tabulated potentials. We used linear dimensions of $L = 60$, 90, 120 and 180, equilibrated carefully, and needed a statistical effort of up to 1 500 000 MC sweeps over the lattice. Since the relaxation time at T_0 even for $L = 180$ is estimated to be not larger than $\tau \sim 50\,000$, our observation time by far exceeds the relaxation time.

From the plateau, we obtain $2/\xi$ directly and plot ξ^{-1} in Fig. 1. as a function of temperature. The behavior of ξ^{-1} demonstrates that the correlation length increases upon approaching T_0 but without showing even an onset of a divergence upon coming close to T_0; it should be noted that we managed to measure ξ as close as only 2% (0.3%) off T_0, and that we covered roughly one decade in reduced temperature both from above and below. The temperature dependence of the data suggests extrapolating ξ^{-1} linearly which yields a *finite* $\xi_+ \approx 23$ ($\xi_- \approx 12$) upon approaching T_0 from above (below). Thus, judging from the behavior of ξ we find that the herringbone transition of the APR model is a weak first-order transition. For comparison we have also fitted our $\xi^{-1}(T)$ data to the power law (including the known critical exponent [26] and amplitude

ratio [27]) expected for the $q = 3$ Potts model in 2D. But, as can clearly be seen from Fig. 1. that, especially near T_0, the critical fit is not at all satisfactory.

B. Quantum Effects on the Orientational Phase Transition

We address now the problem to *quantify* the effect of *quantum fluctuation* on the orientational ordering in this molecular system. A method suited to study finite-temperature many-body quantum systems is the *Path Integral Monte Carlo* (PIMC) technique. A very efficient PIMC scheme [28] especially tailored to simulate rotational motion is used to study a many-body system [21]. This allows us to investigate a ***highly realistic*** adsorbate composed of as many as $N = 900$ quantum N_2 rotators and Trotter dimensions up to $P = 500$. Thus we are able to quantify the influence of quantum fluctuations on a collective phenomenon in a *molecular* system beyond strongly simplified models or MF-like approximations.

Following our aim, we try to capture as much of the microscopic features of the system as possible, but restricting ourselves at the same time to design a model which is *just tractable* with modern techniques. First of all, we pin the molecular centers of mass on a regular trigonal $\sqrt{3}$-superlattice found experimentally [19]. In addition, it is established by several methods that the molecular axes stay *in* the graphite plane with a very sharp distribution around this favored plane nearby and below the orientational transition. Concerning the N_2-N_2 interactions, the $X1$ model [29] consisting of site-site Lennard-Jones and quadrupole interactions was shown to yield a realistic representation; the rotational constant Θ_{N_2} was 2.9 K. Steele's Fourier-representation [30] is used to model the N_2-graphite interactions.

The herringbone order parameter (OP) $\Phi = \langle [\sum_{\alpha=1}^{3} \Phi_\alpha^2]^{1/2} \rangle$ is defined [21] with suitably generalized components for PIMC investigations

$$\Phi_\alpha = \frac{1}{NP} \sum_{j=1}^{N} \sum_{s=1}^{P} \sin(2\varphi_j^{(s)} - 2\eta_\alpha) \exp[i\mathbf{Q}_\alpha \mathbf{r}_j] \ , \tag{11}$$

where $\mathbf{Q}_1 = 2\pi(0, 2/\sqrt{3})/a'$, $\mathbf{Q}_2 = 2\pi(-1, -1/\sqrt{3})/a'$, $\mathbf{Q}_3 = 2\pi(1, -1/\sqrt{3})/a'$ and $\eta_1 = 0$, $\eta_2 = 2\pi/3$, $\eta_3 = 4\pi/3$; $a' = \sqrt{3}a$ and $a = 2.46\mathring{A}$.

The central quantity is the OP as a function of temperature, see fig. 2.. The critical temperature T_c of the classical system can be located around 38 K. At high temperatures, the quantum curve of the OP merges on the classical curve, whereas it starts to deviate below T_c. Qualitatively, quantum fluctuations lower the ordering and thus the quantum OP is always smaller than the classical counterpart. The inclusion of quantum effects results in a nearly 10% lowering of T_c, see fig. 2..

Furthermore, we can infer *quantitatively* from our data in fig. 2. that the quantum system cannot reach the maximum herringbone ordering even at extremely low temperatures: the quantum librations depress the saturation value by 10%. In fig. 2., we also compare in detail OP and total energy as obtained from the full quantum simulation with standard *approximate theories* valid for low and high temperatures. One can clearly see how the quasiclassical Feynman–Hibbs curve matches the "exact" quantum

data above 30 K. However, just below the phase transition, this second order approximation in the quantum fluctuations fails and yields *uncontrolled* estimates: just below the point of failure it gives classical values for the OP and the herringbone ordering even *vanishes* below 5 K. On the other hand, the quasiharmonic theory comes from the other end of the temperature axis and yields very accurate data below 5 K.

Our technique also allows to extract an average zero-point libration amplitude of 14° which compares favorably to the 18° from quasiharmonic lattice-dynamics [31] for $X1$-N_2 at 0 K in three dimensions. Since the validity of such approximations is very difficult to estimate *a priori*, exact full quantum *reference* simulations as presented here are clearly required to control such approximation schemes. This becomes clear when one considers the shift in T_c as obtained from the second order Feynman–Hibbs simulation: it breaks down essentially at the same temperature where the transition occurs and a breakdown at a slightly higher temperature would give wrong results. In addition, one does not know where to match the regimes where different approximations are still valid. The PIMC simulations, however, yield exact results over the *whole* temperature range from the classical to the quantum regime.

IV. Random-field induced rounding of the Ising-type transition in physisorbed $(CO)_{1-x}(N_2)_x$ mixtures

The statistical thermodynamics of systems with randomly quenched disorder is a real challenge for theory, for an overview see ref. [32] and references therein. Particularly striking phenomena are predicted in reduced dimensionality, such as the destruction of long-range order of Ising type systems in $d = 2$ dimensions by arbitrarily weak random fields [33]. This absence of true long-range order also shows up in a rounding of the transition even by very weak random fields, which has been confirmed by a recent experiment on $(CO)_{1-x}(N_2)_x$ [34].

Very weak dilution of CO with N_2 molecules (concentrations of 3% or less) produce a strong rounding of the specific heat anomaly of the transition [34]. Assuming that the quadrupole moment and dipole moment of the CO molecules are linearly coupled, one would obtain from the quadrupole–quadrupole interaction between N_2 and CO an effective random field acting on the CO dipole moments. Note that we do not imply, of course, that interactions of any electrostatic origin dominate – van der Waals forces between the atoms may lead to pseudodipolar or pseudoquadrupolar terms as well. For simplicity we describe the system by a simple square lattice, disregarding the actual sublattice structure. Associating an Ising spin $S_i = \pm 1$ with a CO molecule at site i and $S_i = 0$ with an N_2 molecule at the site, we arrive at the following Hamiltonian [32]:

$$H = + \sum_{<i,j>} J S_i S_j - \sum_{<i,j>} J' S_i (1 - S_j^2) \tag{12}$$

Here J is the interaction between the nearest neighbour pairs of spins (pseudo–dipole–dipole interaction), J' the hypothetical pseudo-dipole–quadrupole interaction. In this model the sites j taken by N_2 produce a field randomly, sometimes on a site in the sublattice where the spins are up and sometimes in the sublattice where the spins are

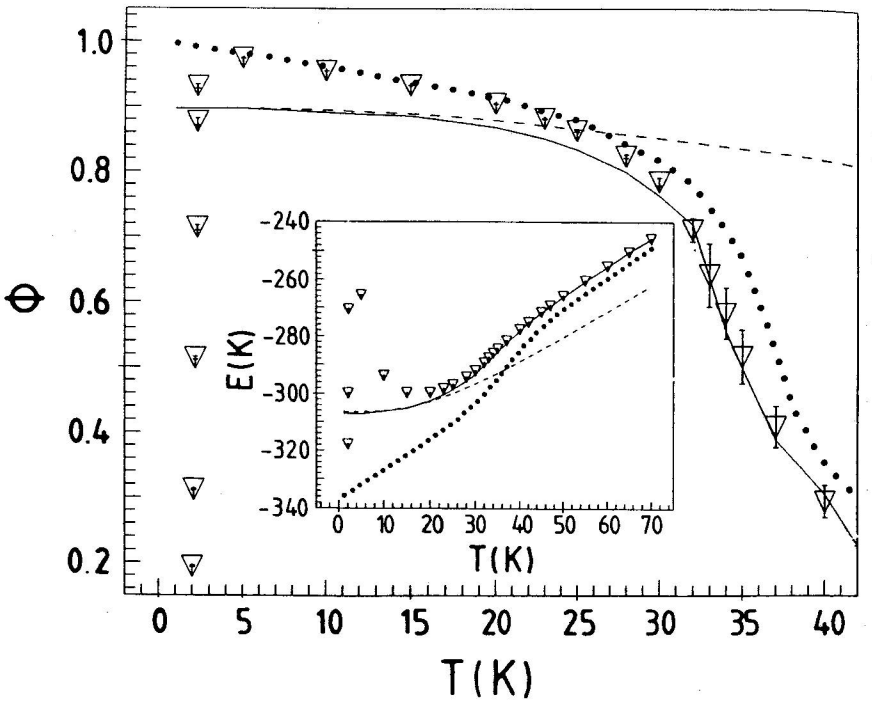

Fig. 2. Herringbone order parameter and total energy for N_2 ($X1$ model with Steele's corrugation). Quantum simulation, full line; classical simulation, dotted line; quasiharmonic theory, dashed line; Feynman–Hibbs simulation, triangles. The lines are linear connections of the data.

down. This model is studied by Monte Carlo methods [32]. We used square lattices of sizes $L = 24, 32, 40, 50$ with periodic boundary conditions and different impurity concentrations x. Averages are taken over $100 - 200$ different configurations of the impurity distribution over the lattice for each x. Typically, systems were equilibrated with runs of a duration of 2.5×10^4 MCS per site, while averages are taken over the subsequent period of 2.5×10^4 MCS/spin, all computations were done on IBM RISC 6000/320 workstations. Figure 3. shows the rounding of the specific heat for different impurity concentrations. Detailed analysis of the order parameter, susceptibility and the cumulant [32] are consistent with the interpretation that the transition in the pure system is rounded by the random field.

Following Fishman and Aharony [35] the crossover from the critical behavior of the pure system ($x = 0$) to the new behaviour can be described by a scaling theory. Just as there is a scaling behaviour with a uniform ordering field h' in a pure system, $C = |t|^{-\alpha}\tilde{C}_{h'}(th'^{-\Delta})$, where $t = 1 - T/T_C$ and $\Delta = \gamma + \beta$, and α, β and γ are the standard critical exponents of specific heat, order parameter and susceptibility, there is a similar scaling with the random field amplitude h in the random field Ising model,

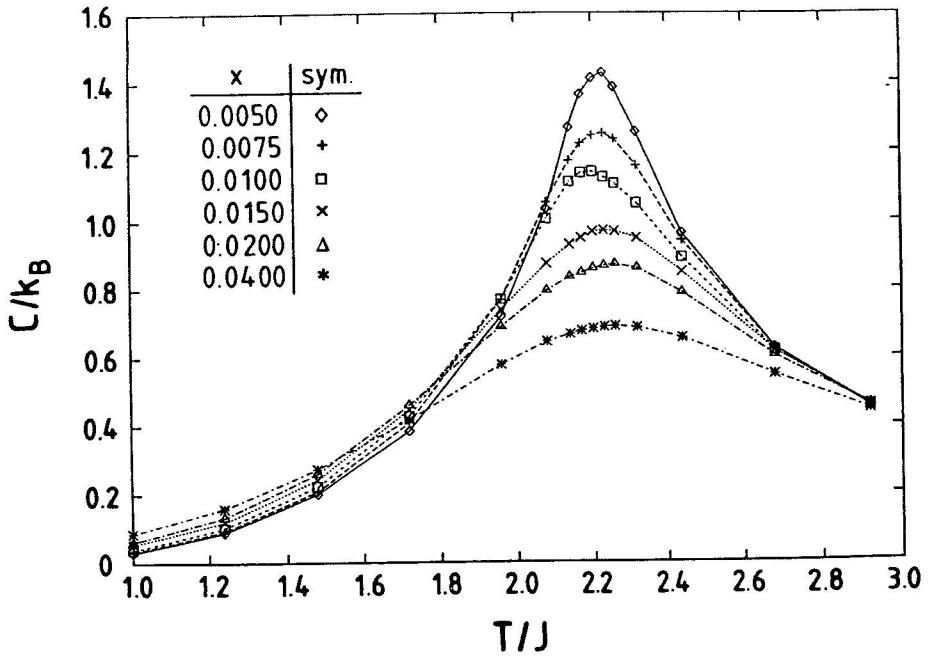

Fig. 3. Specific heat C per lattice site plotted versus T/J for $L = 50$ and various choices of x as indicated, data for J'/J = 2.

namely $C = |t|^{-\alpha}\tilde{C}_h(th^{-2/\phi})$, where the crossover exponent $\phi = \gamma$. The logarithmic specific heat divergence implied by $\alpha = 0$ actually means that additional logarithmic terms are needed,

$$C = \tilde{C}_h(th^{-2/\phi}) - (2A/\phi)\ln h \tag{13}$$

for $t \to 0$, $h \to 0$, $|t|h^{-2/\phi}$ finite, where A is the known specific heat amplitude of the pure system. Now the problem arises of how we can translate the randomness of our Hamiltonian to the random field considered in the theory. The standard assumption is that one simply equates the configurationally averaged moments, noting that for an antiferromagnet we need to consider a random staggered field rather than a random uniform field. Due to the phase factor $(-1)^{l+k}$, where l, k are the x, y coordinates of the lattice site i, the random staggered field acting on site i due to the second term in the Hamiltonian is $h_i = (-1)^{l+k}J'\sum_j(1 - S_j^2)$, $[h_i]_{av} = (-1)^{l+k}J'zx$, z being the coordination number of the lattice, remembering that the sum over j runs over nearest neighbours only. After averaging over the lattice sites, $[h_i]_{av}$ vanishes due to the phase factor. However, for h_i^2 we find $h_i^2 = J'^2\sum_j(1 - S_j^2)\sum_{j'}(1 - S_{j'}^2)$, $[h_i^2]_{av} - [h_i]_{av}^2 = J'^2z^2x(1 - x)$. From this consideration one may identify the random field amplitude h as $zJ'\sqrt{x(1-x)}$. We thus expect $C_{max} = constant - (A/\phi)\ln[x(1 - x)]$. Our data

are nicely compatible with a logarithmic variation, however the constant in front of the logarithm is a factor 1.5 too large, compared to the theoretically predicted one. We attribute this to our numerical limitations (critical slowing down and finite-size effects prevented us from the study of somewhat smaller x). We also analyzed the scaling function $C^*[t(h/J)^{-8/7}]$ with $C^* = C + A^* \ln(h/J)$ and $t = (T/T_m - 1)$, T_m is the temperature of the specific heat maximum, $h/J = \sqrt{x(1-x)}$, and reasonable confirmation of crossover scaling is obtained.

For the case of pure CO-adsorption ($x = 0$) we investigated [36] the low temperature ordering of CO physisorbed on graphite, by Monte Carlo simulations with finite-size scaling methods using a realistic microscopic model with continuous orientational degrees of freedom and a recent *ab initio* potential. Based on the finite-size scaling behavior of the order parameter- and energy-cumulants, the order parameter and its susceptibility, the head-tail ordering transition of CO on graphite is assigned to the 2D Ising universality class. This assignment as well as the critical amplitude of the heat capacity agrees with recent experiments [34]. Quantum fluctuations do not alter the ground state order but rather renormalize the low critical temperature by -10%. In addition to the confirmation of the experimental findings which rests on a much broader basis, we go beyond experiments and predict [36] further details such as the critical amplitude of the order parameter. An analysis of different contributions constituting the total CO-CO interactions reveals that the ordering is not caused by the electrostatic dipole moment, but by the shape-asymmetry of the molecule. We suggest that the ordered ground state is a ferrielectric herringbone structure with a net dipole moment perpendicular to the herringbone symmetry axis.

V. Summary

Phase transitions in adsorbed layers are studied by Monte Carlo and density functional techniques. In the case of the entropy driven phase separation of a nonadditive symmetric hard disc fluid we locate by a combination of GEMC with finite size scaling techniques the critical line of nonadditivities as a function of the system density, which separates the mixing/demixing regions, we compare with a simple approximation. We successfully combine path integral Monte Carlo (PIMC) and GEMC techniques in order to locate the gas-liquid coexistence densities for a fluid with classical degrees of freedom and internal quantum states, good agreement with NVT-ensemble results is obtained, the predictions of density functional- and mean field are presented. Linear N_2 molecules adsorbed on graphite (in the $\sqrt{3} \times \sqrt{3}$ structure) show a transition from a high temperature phase to a low temperature phase with *herringbone* ordering of the orientational degrees of freedom. The order of the transition is determined in the anisotropic planar rotor model by analysis of the correlation length ξ near the transition temperature T_0. The simulation data, extrapolated to T_0, yield a large but finite ξ at T_0 demonstrating that the herringbone ordering is a weak first order transition. The effect of quantum fluctuations on the herringbone transition is quantified by PIMC and classical simulational methods. Quasiclassical and quasiharmonic calculations agree for high and low temperatures, respectively, but only PIMC gives satisfactory results over the entire temperature range. The random-field-induced rounding of the Ising-type transition in physisorbed $(CO)_{1-x}(N_2)_x$ mixtures can be understood in terms of a simple Ising type model. Good qualitative agreement is obtained with recent experiments.

Acknowledgements: Discussions and cooperation with K. Binder, M.O. Ihm, D. Marx, O. Opitz, V. Pereyra F. Schneider, S. Sengupta and H. Wiechert and financial support from the Deutsche Forschungsgemeinschaft (Heisenberg Fellowship) are gratefully acknowledged as well as the granting of computer time on the Cray-YMP (HLRZ Jülich and RHRK Kaiserslautern), VP 100 (RHRK Kaiserslautern), and IBM RISC System/6000 cluster (ZDV Mainz).

References

[1] *Ordering in Two Dimensions* edited by S. K. Sinha (North- Holland, Amsterdam, 1980).

[2] *Phase Transitions and Critical Phenomena* Vol.11 edited by C. Domb and J. L. Lebowitz (Academic, London, 1987).

[3] *Phase Transitions in Surface Films 2* edited by H. Taub, G. Torzo, H. J. Lauter, and S. C. Fain Jr. (Plenum, New York, 1991); *Excitations in 2-D and 3-D Quantum Fluids* edited by A. F. G. Wyatt and H. J. Lauter (Plenum, New York, 1991).

[4] T. Biben, J.P. Hansen, Phys. Rev. Lett. **66**, 2215 (1991); J. G. Amar, Mol.Phys. **67**, 739 (1989); D. Gazillo, G. Pastore, Chem. Phys. Lett. **159**, 388 (1989).

[5] A.Z. Panagiotopoulos, Mol. Phys. **61**, 813 (1987); Molec. Silmul. **9**, 1 (1992).

[6] K. Binder, Z. Phys. **B 43**, 119 (1981); M. Rovere, D.W. Heermann, K. Binder, Europhys. Lett. **6**, 585 (1988).

[7] F. Schneider, M.O. Ihm, P. Nielaba, in *Computer Simulation Studies in Condensed Matter Physics VII* edited by D.P. Landau, K.K. Mon and H.B. Schüttler (Springer, Berlin, 1994) in press.

[8] M.-O. Ihm, Diplomarbeit, Mainz 1993.

[9] T.W. Melnyk, B.L. Sawford, Mol. Phys. **29**, 891 (1975).

[10] F. Schneider, Dissertation, Mainz.

[11] P. de Smedt, P. Nielaba, J.L. Lebowitz, J. Talbot, L. Dooms, Phys. Rev. **A38**, 1381 (1988).

[12] D. Marx, P. Nielaba, K. Binder, Phys. Rev. Lett. **67**, 3124 (1991); Phys. Rev. **B 47**, 7788 (1993).

[13] K.K. Mon, K. Binder, J. Chem. Phys. **96**, 6999 (1992).

[14] S. Sengupta, D. Marx, P. Nielaba, Europhys. Lett. **20**, 383 (1992).

[15] T.V. Ramakrishnan, M. Yussouff, Phys. Rev. **B19**, 2775 (1979); see also A.D.J. Haymet, D.J. Oxtoby, J. Chem. Phys. **74**, 2559 (1981).

[16] C. Ebner, H.R. Krishnamurthy, R. Pandit, Phys. Rev. **A 43**, 4355, (1990).

[17] Y. Rosenfeld, Phys. Rev. **A 42**, 5983 (1990).

[18] A.C. Mitus, D. Marx, S. Sengupta, P. Nielaba, A.Z. Patashinskii, H. Hahn, J. Phys.: Condensed Matter **5**, 8509 (1993).

[19] M. H. W. Chan, A. D. Migone, K. D. Miner, and Z. R. Li, Phys. Rev. B **30**, 2681 (1984).

[20] O. Opitz, D. Marx, S. Sengupta, P. Nielaba, K. Binder, Surf. Sci. **297**, L122 (1993); O. Opitz, Diplomarbeit, Mainz 1993.

[21] D. Marx, O. Opitz, P. Nielaba, and K. Binder, Phys. Rev. Lett. **70**, 2908 (1993); D. Marx, S. Sengupta, P. Nielaba, J. Chem. Phys. **99**, 6031 (1993).

[22] O. G. Mouritsen and A. J. Berlinsky, Phys. Rev. Lett. **48**, 181 (1982).

[23] O. G. Mouritsen, Chapter 5.3 of *Computer Studies of Phase Transitions and Critical Phenomena* (Springer, Berlin, 1984).

[24] W. Selke, Physica A **177**, 460 (1991).

[25] S. Sengupta, O. Opitz, D. Marx, and P. Nielaba, Europhys. Lett. **24**, 13 (1993).

[26] F. Y. Wu, Rev. Mod. Phys. **54**, 235 (1982).

[27] V. Privman, P. C. Hohenberg, and A. Aharony, in *Phase Transitions and Critical Phenomena Vol. 14* edited by C. Domb and J. L. Lebowitz (Academic, London, 1991).

[28] D. Marx and P. Nielaba, Phys. Rev. A **45**, 8968 (1992).

[29] C.S.Murthy, K.Singer, M.L.Klein, I.R.McDonald, Mol. Phys. **41**, 1387 (1980).

[30] W. A. Steele, Surf. Sci. **36**, 317 (1973).

[31] S. E. Roosevelt and L. W. Bruch, Phys. Rev. B **41**, 12236 (1990).

[32] V. Pereyra, P. Nielaba, K. Binder, J. Phys.: Condensed Matter **5**, 6631 (1993).

[33] Y. Imry, S.K. Ma, Phys. Rev. Lett. **35**, 1399 (1975); K. Binder, Z. Phys. **B 50**, 343 (1983).

[34] H. Wiechert and St.–A. Arlt, Phys. Rev. Lett. **71**, 2090 (1993).

[35] S. Fishman and A. Aharony, J. Phys. C: Solid State Phys. **12**, L729 (1979)

[36] D. Marx, S. Sengupta, P. Nielaba, K. Binder, Phys. Rev. Lett. **72**, 262 (1994).